UNIVERSITY OF CENTRAL OKLAHOMA
Edmond, Oklahoma
College of Graduate Studies and Research

INTERISTITIAL LASER IMMUNOTHERAPY FOR TREATMENT OF METASTATIC CANCER

A THESIS

SUBMITTED TO THE GRADUATE COLLEGE

In the fulfillment of the requirements

For the degree of

MASTER OF SCIENCE IN ENGINEERING PHYSICS

By

Chet Raj Joshi

Edmond, Oklahoma

2011

INTERISTITIAL LASER IMMUNOTHERAPY FOR TREATMENT OF METASTATIC CANCER

A THESIS

APPROVED FOR THE DEPARTMENT OF ENGINEERING PHYSICS

05/03/2011

Thesis Approved by:

Chair of Advisory Committee

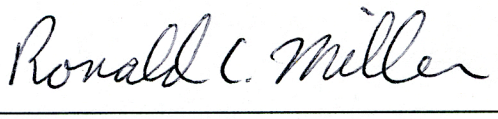

Committee Member

Committee Member

Acknowledgements

I would like to express my sincere thanks to my thesis advisor, Dr. Wei R. Chen, for his continued support, constant encouragement and guidance in completing this project. In addition, I would like to thank the Department of Engineering Physics at the University of Central Oklahoma for providing me with the opportunity to work on my master's degree. I would also like to thank my thesis Advisory Committee members for their valuable advice throughout the degree program. I am thankful to my friend Mandip Aryal for his continuous support and encouragement, and I am grateful to my wife Raksha Ojha for her incredible support and understanding. I appreciate my research collaborators for their contribution of time and knowledge to this project. I would like to extend my sincere thanks to the Oklahoma Medical Research Foundation and the University of Oklahoma Health Sciences Center for providing the facilities and technical assistance for my experiments. Finally I want to thank to all the people who have helped me directly or indirectly in completing this project.

TABLE OF CONTENT

LIST OF FIGURES & TABLES

Section 2

Section 3

Section 4

Abstract

Cancer is one of the leading causes of death in the world. Although widely used, currently available cancer treatment modalities such as surgery, chemotherapy and radiation have limited effects in curing the disease and prolonging the life of late-stage cancer patients. A novel therapy, laser immunotherapy (LIT) has been developed for the treatment of late-stage metastatic cancers. LIT uses laser light to kill cancer cells and a non-toxic immunoadjuvant, glycated chitosan (GC) to stimulate the host immune system. It fights against residual tumor cells, as well as metastases at distant sites. LIT is a combination of photothermal therapy and immunotherapy. The current application of LIT is non-invasive, using light to penetrate surface skin tissue to treat underlying tumor cells. Modifications to the LIT treatment are necessary to effectively treat patients with pigmented skin and deep tumors. Thus, interstitial laser immunotherapy (ILIT), using an invasive laser irradiation approach, is proposed. The present study is designed to investigate the effectiveness of ILIT using an 805-nm laser. DMBA-4 metastatic mammary tumor cells line in Wistar Furth female rats was used. Irradiation of rat tumors was performed using an interstitial fiber with a cylindrical diffuser. The temperature distribution inside the target tumor tissue, an important factor affecting the outcome of ILIT, was monitored with a thermocouple by inserting needle probes into the tissue around the cylindrical diffuser during laser irradiation. To measure the three-dimensional temperature distribution in the target tissue, the proton resonance frequency (PRF) method was conducted using a 7.1-Tesla magnetic resonance imager. Our results showed that the temperature distribution in tissue depended on laser power and irradiation duration. The temperature inside the target tumor varied with the distance from the laser diffuser tip. Thermal damage to the tumor was examined using triphenyltetrazoium chloride (TTC) staining as well as hematoxolin and erosion (H&E)

staining. Animal survival as well as tumor size over time was monitored. Our results indicate that ILIT had a much greater thermal impact on target tumors with less surface damage than LIT. The survival study also indicates that ILIT has better potential for treating metastases and deep tumors, while having fewer side effects than LIT.

Keywords: Laser immunotherapy, interstitial laser irradiation, immunoadjuvant, cancer treatment, thermal damage, proton resonance frequency, rat tumor, DMBA-4 cell line, cylindrical diffuser, tissue temperature elevation, magnetic resonance imaging.

1. Introduction

Cancer is the second leading cause of death in the world, after heart disease. According to the U.S. National Cancer Institute, “Cancer is a term used for diseases in which abnormal cells divide without control and are able to invade other tissues”. Cancer normally spreads to other parts of the body through blood and lymph node systems. Cancer cells differ from normal cells in many physiological conditions, such as cytoskeletal changes, cell adhesion/motility, nuclear changes, and enzyme production. Cancer cells often change their appearance and are disorganized abnormally [1-4].

There are thousands of new cancer cases every year. The most common types of cancers are breast cancer, bladder cancer, lung cancer, colon cancer, blood cancer, prostate cancer, and melanoma. In 2010, the most common type of cancer reported was lung cancer with an incident of 222,000 new cases and 157,300 deaths. There were about 40,000 estimated deaths due to breast cancer alone [5-6].

Among all the cancers, metastasis poses the most severe challenge and it is the major cause of treatment failure of cancer patients. The most common treatment modalities for cancer are chemotherapy, radiotherapy, and surgery [7-9]. Chemotherapy is a treatment process that uses anti-cancer drugs, targeting fast splitting cells. In radiotherapy, the controlled dose of radiation is used to directly destroy tumor cells. In surgery, the infected parts are cut away by using a scalpel or laser. Unfortunately, the long-term survival rates with these treatment methods have been low on late-stage challenge to the physicians and researchers.

Facing this challenge, Chen and co-workers developed a novel technique for treatment of late-stage metastatic cancer with a combination of photothermal interaction and immunological stimulation called laser immunotherapy (LIT) [14-16]. LIT is a treatment method which uses the

laser to irradiate target tumors. Laser light interacts with biological tissues in three different ways: photochemical, photothermal, and photomechanical. Photothermal interaction can be an effective way to destroy tumor cells due to the sensitivity of tumor tissues to temperature increase. As the temperature is increased, normal tissue surrounding the target tumors can also be damaged and such damages need to be minimized to reduce the side effects [17-28]. In addition, for the long-term effect, LIT also includes immunological stimulation in combination with photothermal interaction.

LIT has shown to be a promising method of cancer treatment lately. LIT can be considered as an *in situ* autologous vaccine that, through local intervention, uses whole tumor cell as the sources of tumor antigens from each individual patient without *ex vivo* preparation or pre-selection of tumor antigens. LIT, thus represents a new and significantly improved approach using a new and highly potent non-toxic immunoadjuvant, glycated chitosan (GC). Furthermore, the use of laser irradiation also reduces the tumor burden in addition to the release of tumor antigens.

Specifically, LIT uses a near-infrared laser light to generate heat (photothermal interaction) to kill the tumors at specific temperatures and liberate tumor antigens. The injected GC interacts with the liberated tumor antigens to induce an immune response against the cancer [29-34].

Chen and co-workers first proposed the treatment of metastatic tumor using LIT in 1997. Initially, LIT was employed for non-invasive treatment of subcutaneous tumors, using an *in situ* light-absorbing dye. Deeper tumor couldn’t be treated effectively, because the light absorption of the tissue between the skin and the targeted tumor prevented sufficient laser energy from reaching the tumor. To overcome the limitations of LIT, interstitial laser immunotherapy (ILIT)

is developed using an optical fiber with cylindrical diffuser for the treatment of deep tumors. This is an invasive method that delivers the light directly to the center of the tumor, thus avoiding the attenuation of light due to the intervening tissues between the skin and the tumor.

The response of the tumor and its surrounding normal tissue to the laser-induced heat is crucial in the treatment of cancer. It has been known that temperature increase affects biological response. Since tumor cells are more sensitive to the change in temperature than normal cells, thermal interactions can be used for therapeutic purposes. Between the temperatures of 40 degree to 43 degree Celsius, the cytotoxicity effect takes place in tumor cells than normal cells. The vascular destruction is higher in tumor cells at elevated temperatures because tumor cells have low pH and insufficient presence of oxygen [35-47].

In this study, we treated metastatic mammary tumors in rats using ILIT. We evaluated thermal effects using a near-infrared laser with an active cylindrical tipped interstitial fiber. The temperature measurement of the tissue during ILIT treatment was employed using thermocouple and magnetic resonance therapy (MRI) techniques. The thermocouple provides temperature measurement at a specific point whereas MRI provides a three dimensional temperature distribution. Water proton resonance frequency (PRF) has been used for this purpose. The 3-D presentation of the temperature distribution provides a more comprehensive understanding of the treatment process [48-56].

In pre-clinical studies and preliminary clinical trials for late-stage, melanoma and breast cancer patients, LIT have shown promising outcomes [57-60]. Not only are primary tumors treated successfully, but untreated metastatic tumors at distant sites are eliminated. Prolonged patient survival has been observed in both melanoma and breast cancer patients. In this study, we investigate the overall survival and immune responses of ILIT treatment on rat tumors.

The experiments performed in this study could lay the foundation for future clinical applications of ILIT for the treatment of deep tumors.

2. Theory

2.1 Laser

Laser stands for Light Amplification by Stimulated Emission of Radiation. A laser emits electromagnetic radiation of a monochromatic wave which is amplified as the photons are stimulated. Laser light energy is very concentrated, which is different than other lights produced by other mechanisms.

2.1.1 Properties of Lasers

- The laser light is monochromatic. In this study, we used a near-infrared laser light with a wavelength of 805 nm.
- A laser emits photons. Photons are perfectly aligned with each other and travel at the same speed.
- The photons of the laser light are released from a small opening with high intensity. Therefore, the laser light can be used to direct energy efficiently to the targeted tumor.
- The near-infrared laser light is invisible to the naked eye. In this wavelength range, biological tissue is almost transparent.

2.1.2 Diode Laser

In this study we used a specific type of laser called diode laser. A diode laser is formed by doping a crystal wafer to n-type and p-type regions using impurities. These n and p regions make a p-n junction. The p-n junction is also referred to as the diode. Holes from the p-region and electrons from the n-region are injected into the depletion region due to the differences in

potential between p and n regions. Since the two opposite charges are in the same region, recombination occurs. In this case the electrons and the hole combine to produce photons, which are released with energy equal to the difference between the states of the hole and the electron. This process is referred to as the spontaneous emission of photons. The emission of photons is seen in the form of light.

While this occurs, stimulated emission, electrons and holes go through a process called recombination. During this process, when electrons and holes are close to one another, a photon with energy equal to the recombination energy triggers the stimulated emission by recombination. Because of this another photon is created. This new photon will have the same properties as the first photon. The proton will travel in the same direction and will be in the same phase. This process repeats as long as there is availability of holes and electrons in p and n regions respectively. As more and more charge carriers (holes and electrons) are injected into the depletion region, more and more photons with the same properties are produced. Hence, the stimulated emission of photons can be seen in the form of light referred to as the laser light. Light from a diode laser is monochromatic, focused, and intense.

The construction of the diode laser provides a waveguide, a path for the electromagnetic radiation. Since the waveguide is formed on the crystal wafer, the photons have to pass through a very narrow path. In a diode laser, the two ends of the crystal wafer are cut and made very smooth. As the photons pass through the waveguide, they are reflected from the ends of the crystal. Photons moving in the waveguide cause stimulated emission which produces additional photons. At the same time, there is some absorption of photons causing loss of the light. Laser light is produced when the light is amplified at a rate higher than the amount of photons being absorbed.

Figure 2.1. An 805-nm diode laser.

2.1.3 Optical Properties of Biological Tissue

When considering the interaction between laser light and biological tissue, different optical properties need to be considered. In the interstitial studies we are interested in the absorption and scattering of the laser light. The absorption and scattering properties depend on the wavelength of the light used. Since the laser light is emitted from an extended active tip, it can deliver light to a large area in tissue. The biological response of the tissue depends on this temperature change. The power and duration of the laser light determine the injury level of the tissue. The tissue is primarily comprised of water and blood. This plays an important role in the absorption and scattering of the laser light on the tissue. At 600 nm blood absorption is relatively low and at 1300 nm water absorption starts to increase. Therefore, the wavelength range between 600 nm and 1300 nm is called the optical window for tissue. Specifically, an 805 nm diode laser as shown in Figure 2.1 is used in our study.

2.2 Thermocouple

Thermocouple is a temperature measuring device. The device outputs a voltage which is proportional to the temperature difference. A thermocouple circuit is formed by joining two dissimilar metals. A small current due to Seebeck effect is created across the junction. The current or electro motive force that causes the current is proportional to the temperature of the junction. This small potential generated at the junction, is usually in the millivolt range. The schematic of thermocouple is given in Figure 2.2.

A thermocouple thermometer employs two junctions – hot junction and cold junction. The hot junction is connected to the source of interest which is usually at a higher temperature. The cold junction remains at a reference temperature. The electro motive force (EMF) generated is directly proportional to the temperature difference between two junctions. The EMF to temperature ratio in a standard thermocouple is found to be in the range of 1 to 70 microvolt per degree Celsius (µV/°C). The EMF voltage does not mean the voltage is generated at the junctions of two metals but it is the voltage generated along the portion of the length of the two dissimilar metals that is subjected to a temperature gradient. Because both lengths of dissimilar metals experience the same temperature gradient, the end result is a measurement of the temperature at the thermocouple junction. A table has been established worldwide that shows temperature vs. millivolt output figures for the various accepted thermocouple combinations. The reference table is all based on a reference or cold junction of 32 °F, which is the freezing point of pure water. All manufacturers follow this reference table, which was published in ASTM.

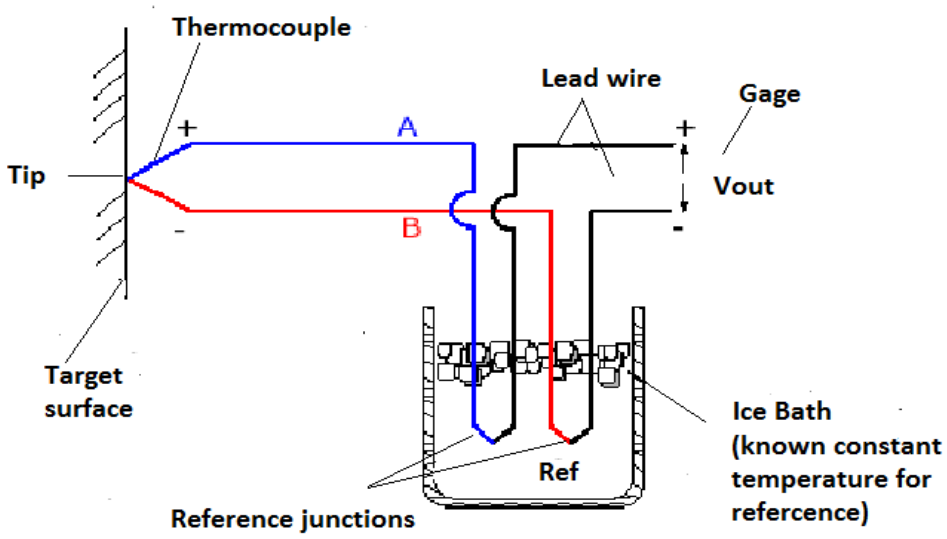

Figure 2.2. Mechanism of Thermocouple.

2.3 Magnetic Resonance Imaging

We used MRI for our study. The MRI technique uses a magnetic field to study the alignment of protons in the targeted tissue. The tissue is mainly made up of water and it has an abundance of hydrogen atoms. Each hydrogen atom has one proton and one electron. In tissue, the protons are randomly oriented, each spinning on its own axis. Even though the protons are charged, they don't act like magnets because of their random orientation. Once the tissue of interest is placed in the MRI machine, a magnetic field is applied and the protons align parallel or opposite to the field lines. These protons are still spinning in their own axis. This movement of magnetic moment of protons is called precession. The angular frequency of the process is given by Larmor equation:

$$\omega = \gamma B. \qquad (1)$$

where ω is angular frequency, γ is gyromagnetic ratio and B is magnitude of the magnetic field.

Then radio frequency (RF) signal is applied to the already magnetized tissue to excite the protons to the upper energy state. The protons precess in a perpendicular direction to the field line. The small magnetic field of each proton adds up to produce a net transverse magnetic field which is detected by the detector coils. The precessing transverse magnetic field produces a changing magnetic field that produces an EMF in detector coils. The strength of EMF depends on the strength of the transverse magnetic field and hence on the number of nuclei contributing to the signal. Once the RF signal is turned off, the protons in the excited state return to the low energy state, releasing energy. This emission of electromagnetic waves, by the protons, after the termination of the RF signal, provides valuable information of the target tissue. The normal tissue and the diseased tissue have different return rates (or relaxation times), thereby differentiating these two types of tissues. The 3-D imaging in MRI is accomplished by using a large set of interactions of one atom with the other and by using RF pulses and delays.

Figure 2.3. A 7.1 Tesla MRI system for small animal studies.

2.3.1 Characteristics of Magnetic Resonance

2.3.1.1 Spin

The nuclear spin quantum number S designates the spin of the nucleus. If the number of protons and neutrons are equal in a given nuclei then S is zero.

2.3.1.2 Spin Angular Momentum

The angular momentum in a nucleus is quantized. It is also called the magnetic quantum number m. The magnitude and orientation of the angular momentum takes the value from –S to +S, giving rise to 2S+1 number of angular momentum states. The z component of the angular momentum vector is given by:

$$S_z = m\hbar, \qquad (2)$$

where $\hbar$ is reduced Planck's constant. Similarly, the z component of the magnetic moment is given as [61-64]:

$$\mu_z = \gamma S_z = \gamma m\hbar, \qquad (3)$$

where γ is the gyromagnetic ratio of the proton.

Spin Behavior in a Magnetic Field

An atom may be neutral when there is no force acting on it. But when an atom or nucleus is placed in an external magnetic field, there is an interaction of this external magnet field with the magnetic moment of the nucleus. The energy of a magnetic moment μ under the influence of a magnetic field B_0 is given by:

$$E = -\mu \,.\, B_0 = -\mu_x B_{0x} - \mu_y B_{0y} - \mu_z B_{oz,} \qquad (4)$$

where μ is the magnetic moment of the proton.

When the magnetic field B_0 is acting along the z-axis,

$$E = -\mu_z B_{0,} \qquad (5)$$

or,

$$E = -\gamma mhB_{0,} \qquad (6)$$

As long as the magnetic field B_0 is not zero, there will be different energies for different spin states. The energy difference between these two states can be found by the following equation [68]:

$$\Delta E = \gamma hB_{0,} \qquad (7)$$

2.3.1.3 Magnetic Resonance by Nuclei

For magnetic resonance by nuclei, the specific level of energy is found by the Larmor equation. The right choice of frequency for the RF signal is important for resonant absorption by nuclear spins. The energy is given by the equation:

$$E = h\nu, \qquad (8)$$

where, h is the plank's constant and ν is the resonant RF which is equal to the frequency as defined by the Larmor equation in a constant magnetic field B_0. This amount of energy creates photons which then will be detected by the nuclear magnetic resonance (NMR) [65-70].

2.3.1.4. Relaxation

The term *relaxation* refers to the nucleus returning to the previous state of net magnetization. When this occurs, the energy difference is emitted in the form of electromagnetic

radiation, a RF signal called the NMR signal. There are two different mechanisms that define the relaxation. They are as follows:

- The longitudinal or spin lattice relaxation time (T1)
- The transverse or spin-spin relaxation time (T2)

T1:

When a spin makes a transition from the high energy state to low energy state, the nucleus tries to come to equilibrium by releasing RF energy into the surrounding lattice. In other words, it is the energy exchange between spin and the lattice.

T1 is also referred to as the recovery time of z component of the nuclear spin magnetization, M_z, coming to equilibrium state as symbolized by $M_{z,eq}$. In general,

$$M_z(t) = M_{z,eq} - [M_{z,eq} - M_z(0)]e^{-t/T1}, \qquad (9)$$

When the spin magnetization vector, M, is inclined to XY plane, then M_z (0) = 0. The new recovery would be then as follows:

$$M_z(t) = M_{z,eq}(1 - e^{-t/T1}), \qquad (10)$$

After one T1 is completed, the longitudinal magnetization returns to 63% of its final value. T1 is dependent on the NMR frequency and the external magnetic field B_o.

T2:

When spins are precessing together, sometimes they interact with each other causing a phase change. This is due to the fact that each spin has its own magnetic field and it interacts with other spins, getting some spins out of phase [71-75].

T2 is referred to as the decay constant of the spin magnetization vector (M) when perpendicular to the magnetic field $B_{0.}$ The component of M is symbolized as $M_{xy.}$ When at time zero, the x-y magnetization will decay to zero as defined by the equation:

$$M_{xy}(t) = M_{xy}(0)(1 - e^{-t/T2}). \qquad (11)$$

After time T2, the transverse magnetization decays to 63% of original value.

T2 is always shorter than T1. T2 is less dependent on the magnetic field strength as compared to T1.

2.4 Laser Immunotherapy (LIT)

LIT is a cancer therapy with the combination of photothermal interaction and immunological stimulation. It induces an anti-tumor immune response for the control of abnormal growth of cells in the treated tumors. In order to increase the absorption of laser light by tumor tissue, indocyanine green (ICG) solution is injected into the tumor before the laser irradiation. ICG has an absorption peak around 800 nm which matches with the wavelength (805nm) of the laser. Due to this increased absorption of the laser with ICG, most of the laser energy is concentrated in the tumor cell. Hence, this increases the temperature of the tumor tissue while keeping the surrounding tissue at a lower temperature to prevent the damage to the normal tissue. When the laser light is focused on the tumor cells for certain duration of time, thermal tissue damage and coagulation occur because of photothermal effect.

2.4.1 Photothermal Response by Biological Tissues

Biological tissues are sensitive to temperature increase. Temperature increases tissue blood flow if it reaches 40^{o}C. Above 41.5^{o}C in tumor cells, cellular cytotoxicity occurs. Above 42.5^{o} C in tumor cells, vascular destruction occurs. For every temperature increase in tumor cells by 1^{o}C beyond 43^{o} C, the cell dies at twice the normal rate. Tumor cells have low oxygen content resulting in a low pH level meaning a more acidic environment. In acidic medium, the cytotoxicity effect of heat is more pronounced and can cause more damage. For this reason, the tumor cells are more sensitive to temperature increase compared to the normal cells. The growth of tumor cells can be controlled by a temperature increase accomplished by using laser irradiation. Heat alone is not sufficient to stop complete growth of tumor cells [76-79].

2.4.2 Immune Response

Photothermal therapy not only kills the tumor cells, but also induces immune response. As the immune response induced by photothermal therapy is regulated by temperature change, controlling heating levels in the tissue provides different modulator effects. The fever-range temperature (39^{o}C-40^{o}C) can modulate antigen presenting cells (APC), T cells and natural killing cells (NK cells). Heat shock temperature range (41^{o}C-43^{o}C) can increase the immunogenicity of tumor cells. Above cytotoxic temperature (43^{o}C), an antigen source is formed which induces an anti-tumor immune response [34]. The antigens so produced could be tumor associated antigens, thermally induced heat shock proteins (HSP), and a large amount of self antigens. Dendritic cells (DC) transfer these antigens to lymph nodes whereas T-cells induce an immune response against tumor cells.

Once the tumor cells are killed, their debris might not be able to transfer or produce enough antigens thereby reducing the anti-tumor immune response. The need for external interventions for anti-tumor immune response can be answered by adding more cytokines to increase the number of DCs [80-81]. There are different cytokines available, which can be used for this purpose depending upon the nature of tumor cells. Granulocyte monocyte colony stimulating factor (GM-CSF), tyrosine kinase 3 ligand (Flt3L) could be used. Similarly, cytotoxic T-lymphocyte antigen 4 (CLTA-4) blocking antibodies and TLR9 ligand provides further anti-tumor immune response [82-86].

2.5 Interstitial Laser Immunotherapy (ILIT)

In ILIT, the tumor cell is targeted directly by inserting laser fiber into the target tissue. The laser light is absorbed directly without the assistant of indocyanine green or other light-absorbing dye. ILIT has several advantages over LIT. LIT uses ICG solution in the middle of the tissue but does not guarantee the uniform distribution of laser light over the tumor tissue. ILIT does not need the ICG solution as the laser fiber is inserted directly into the middle of the tissue. Due to the high absorption of laser light by ICG solution in LIT therapy technique, dark skin patients run the risk of severe skin damage, which in turn can also limit the absorption of laser light by the tumor below the surface tissue. A cylindrical diffuser tip is used in the ILIT technique to deliver the laser light into deeper tissue. The cylindrical diffuser tip spreads the laser light cylindrically to create a larger, more uniform photothermal damage zone inside the tumor.

3. Experiment Setups and Methods

3.1 Introduction

The experiment for the treatment of metastatic mammary tumors in rats was conducted using an 805-nm diode laser. Healthy Wistar Furth female rats were injected with DMBA-4 mammary tumor cells. The tumors were then treated using laser irradiation at different powers. The significance of the laser treatment was determined based on the rat survival rates. Since temperature distribution was the most crucial factor for the treatment, the temperature mapping was carried out using (i) thermocouple for temperature measurement at strategic locations and (ii) MRI for 3-D temperature mapping.

The first experiments were conducted at the University of Oklahoma Health Science Center (OUHSC) for survival studies and thermocouple temperature measurement purposes. Tumor-bearing rats were divided into different groups treated with different laser parameters to study their survival. A power meter was used to measure the laser power output. A fiber optic with a cylindrical diffuser was inserted into the tumor with the aid of needles. For the thermocouple temperature measurement, temperature probes were inserted into the tumor around the cylindrical diffuser fiber tip. Temperature at different distances from the cylindrical diffuser was measured. The treatment was followed by an intratumoral injection of GC. The histology of the tumor tissue was observed using triphenyltetrazoium chloride (TTC) staining.

A second group of experiment was done at Oklahoma Medical Research Foundation (OMRF) for 3- D temperature measurement purpose. The magnetic field strength of the MRI device and the use of near infrared laser light were selected appropriately. The treatment protocols for the devices used are described in detail below.

3.2 Near Infrared Laser and Optical Fiber with Cylindrical Diffuser

Near-infrared light was delivered using an 805-nm diode laser (Delta-30 AngioDynamics, Queensbury, NY) with a maximum power output of 30 watts as shown in Figure 2.1. The laser light was delivered interstitially using a cylindrical diffuser fiber tip. As shown in Figure 3.1, the diffuser fiber has a 1-cm active tip (Pioneer Optics, Bloomfield, CT). Output power was measured using a power meter (Ophir-Spricon, Logan, UT) as shown in Figure 3.2 before and after each tumor irradiation.

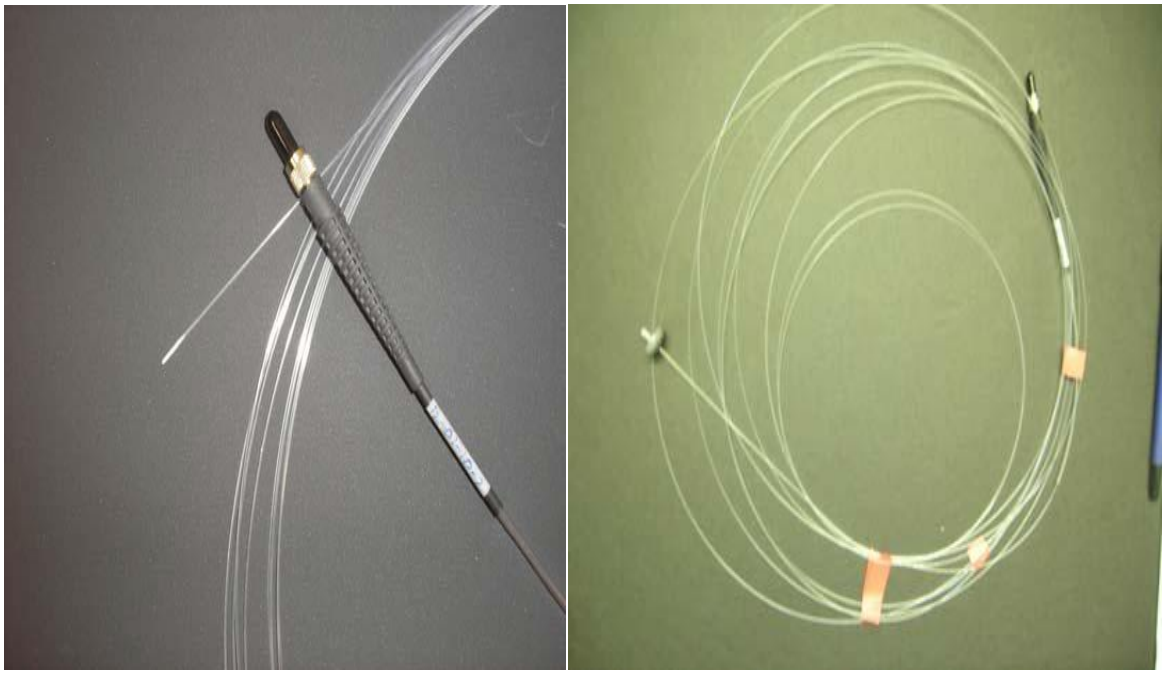

Figure 3.1. Optical fiber with a) 1 cm cylindrical diffuser b) 0.5 cm cylindrical diffuser.

Figure 3.2. A power meter.

3.3 Preparation of Tumor for Interstitial Irradiation

DMBA-4 metastatic mammary tumor cells (100,000 cells per rat) were injected into the upper back part of Wistar Furth female rats. Tumors were left to grow until the size of 1.0-1.5cm was reached, usually in approximately 7-10 days after tumor inoculation. These tumors were then irradiated by the laser using an optical fiber as shown in Figure 3.3. Laser irradiation was followed by 0.2 ml of immunoadjuvant GC.

3.4 Experiment Setup for Survival Study

A total of 91 rats were divided into 7 different groups, as shown in Table 3.1. The survival of rats with metastasis over time was observed.

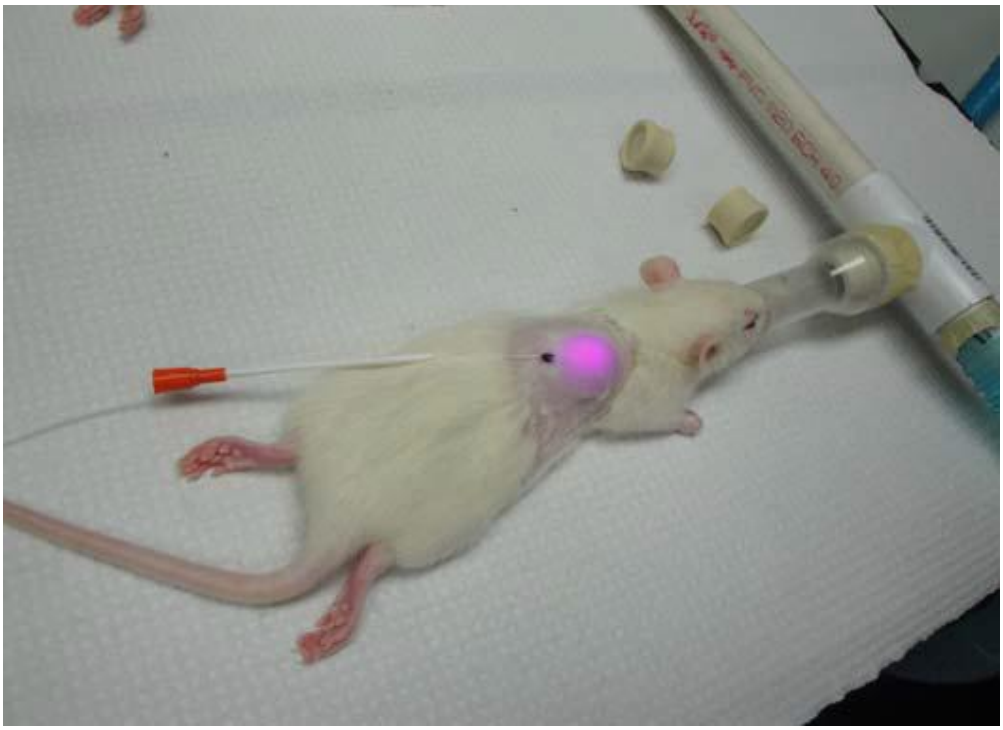

Figure 3.3. Irradiation of rat tumor with a cylindrical diffuser placed inside the tumor.

Table 3.1 Rat Experiment Group

Group #	**Treatment**	**Number of Rats**
Group 1	Control	9 rats
Group 2	1W/cm^2 for 10 min	14 rats
Group 3	1.5 W/ cm^2 for 10 min	14 rats
Group 4	2W/ cm^2 for 10 min	14 rats
Group 5	2.5 W/ cm^2 for 10 min	14 rats
Group 6	3W/ cm^2 for 10 min	14 rats
Group 7	2W/ cm^2 for 30 min	14 rats

3.5 Experimental Setup for Thermocouple Measurements

Two rats from each experimental group were selected for thermocouple measurement. For temperature measurement, each rat was allowed to lie on its stomach during irradiation. The thermocouple probes were positioned at a distance of 0.2 cm and 0.5 cm from the laser fiber tip.

Before the experiments were performed, the thermocouple was calibrated on InstruNET software (Omega Engineering, Stamford, CT) using freezing and boiling bathes at 0^0C and 98^0C as reference points.

3.6 Experimental Setup for 3-D Temperature Determination

Rats were treated with three different laser settings: (i) 1.6W for 10 min, (ii) 2.2W for 10 min and (iii) 1.8W for 30 min. Incisions on the tumors were made using a 14-gauge needle. Laser light was delivered to the tumor by inserting the optical fiber with a 0.5 cm cylindrical active tip into the tumor guided by the pre-inserted 14 gauge needle. The rat was placed inside a commercially made acrylic tube. This tube was then placed inside MRI machine. Anesthesia was used on rats to acquire a constant breathing rate of 35 breaths per minute.

3.6.1 PRF Calibrations and Validation

Calibration on proton resonance frequency (PRF) method was done using chicken breast as a reference tissue. The chicken breast was cooled to 0^oC overnight in an ice bath. Measurements using fiber optic sensors (FISO Technologies, Quebec, Canada, +/-0.5^oC) were used as a reference.

Ex vivo bovine liver tissue was used to test our laser system and the PRF method. PRF was used to measure bovine liver tissue temperature profiles during 10-minute of laser irradiation with 1.5W using the 1-cm active cylindrical tip.

3.7 MRI Method and Configuration

In MRI method, the tissue temperature was determined using MRI phase measurement. The following equation determines the relation between the temperature change and the phase.

$$\Delta T \frac{\Delta \phi}{\gamma B_o \alpha TE} \Delta T = \frac{\Delta \phi}{\gamma B_0 \alpha TE}, \qquad (12)$$

where ΔT is the change in temperature, $\Delta \phi$ is the change in phase, γ is the proton gyro-magnetic ratio, α is the thermal coefficient, and TE is the echo time.

The MRI experiment was accomplished with a 7.1-T MR imaging system (Para Vision 5.0 Software, Bruker BioSpin MRI GmbH, and Germany) as shown in Figure 2.3. A fast low angle shot (FLASH) gradient-echo (GE) pulse sequence was used. The value of the echo time (TE) was 4 ms and that of the repetition time (TR) was 200 milli second. The scans were gated in this case so as to avoid the artifacts caused by motion due to respiration. Hence temporal resolution was calculated by taking the average of total elapsed time over the total number of cycles.

For the MRI settings on the rats, ten slices (1 mm thickness) were selected along the 0.5 cm length of the active cylindrical tip. Spatial resolution was set to 128X128 pixels whereas FOV (field of view) for 50X50 mm. With all these settings, it was estimated that an MRI machine would run at least 20-35 cycles to achieve the desired resolution. This took approximately 20-40 min. As described in section 3.6, the tumor was irradiated for two different

durations: two groups for 10 minute and one for 30 minute. In each of these three experiments, the tumor samples were imaged for 5 min before laser irradiation began and 5 min after laser irradiation ended.

Similar procedures were followed for the bovine liver experiment with some minor changes. Nineteen slices (1 mm thickness) were used along the 1 cm length of active cylindrical tip. The field of view (FOV) setting was changed to 60X23 mm.

3.7.1 Image Processing

Using the real (Re_n) and imaginary (Im_n) parts of the raw MRI data, the phase difference ($\Delta\phi$) between the phase at frame number n (ϕ_n) and the initial phase (ϕ_o) at a given point was calculated using the following equation.

$$\Delta\phi = \phi_n - \phi_0 = ArcTan\left(\frac{\mathrm{Re}_n\,\mathrm{Im}_0 - \mathrm{Re}_0\,\mathrm{Im}_n}{\mathrm{Re}_0\,\mathrm{Im}_n + \mathrm{Re}_n\,\mathrm{Im}_0}\right). \quad \frac{Re_n Im_o - Re_o Im_n}{Re_o Re_n + Im_o Im_n}$$

(13)

Afterwards, the temperature elevation was obtained from the phase-temperature relation using equation (12). Temperature maps were obtained using MatLab 2008 version 7.6 (The Math Works Inc, Boston, MA).

3.8 Observation of Tissue Damage Using Triphenyltetrazoium Chloride (TTC) Tissue Staining and Histology

To assess tumor tissue viability after interstitial laser irradiation, TTC staining was used. TTC uses dehydrogenises enzyme and cofactor based reaction that converts the tetrazolium salt

to Formosan pigment within viable tissues, which turn the viable tissue from colorless to red-maroon color. Thermal necrotic tissues lack intact enzymatic activities to metabolize the tetrazolium salt therefore do not stain and remain their native color.

Rat tumor without laser treatment was used as control. Three hours after the treatment, the entire tumor with overlying skin was collected. The samples were then sliced under room temperature while remaining wet. The collected tissue samples were immersed into the TTC solution for an hour and then the TTC staining of the tumor was observed. Photographs were taken for both control and laser treated tumor samples before and after TTC staining for comparison.

4. RESULTS

4.1 MRI Temperature Measurements

4.1.1 Calibration of PRF with Chicken Breast Tissue

Calibration of PRF was performed with the standard value obtained from the optical fiber sensors (FISO Technologies, Quebec, Canada, +/-0.5C). At first the laser irradiation was done on the chicken tissue at few specific locations. Temperatures of these locations were obtained directly from the sensors. Then the temperatures of the same locations were found by using the image obtained from PRF and applying equation 9. The readings from optical fiber sensors and PRF were consistent for the first 20 min as shown in Figure 4.1

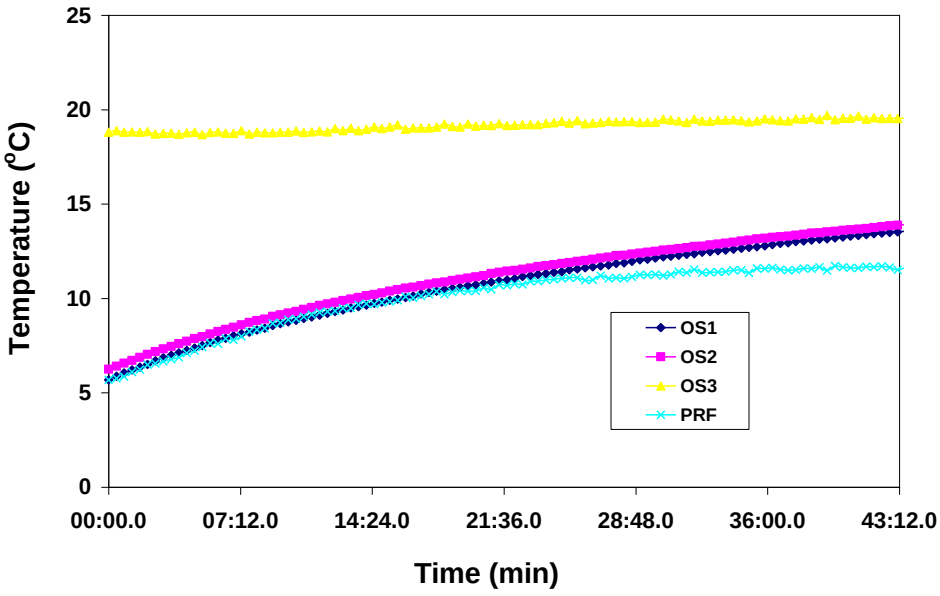

Figure 4.1. Internal temperature of chicken breast tissue measured during calibration. Temperature measured using PRF matches with that of the optical sensors for the first 20 minutes before drifting occurs. Three optical sensors (OS1, OS2 and OS3) were used.

4.1.2 Temperature Profile of Bovine Liver Tissue during Laser Irradiation

Nineteen 1-mm slices of bovine liver were partitioned along the 1 cm active cylindrical tip. Figure 4.2 is the temperature profile of the liver extracted from the 7th to 9th slice. The maximum elevation of temperature was 35 degree Celsius.

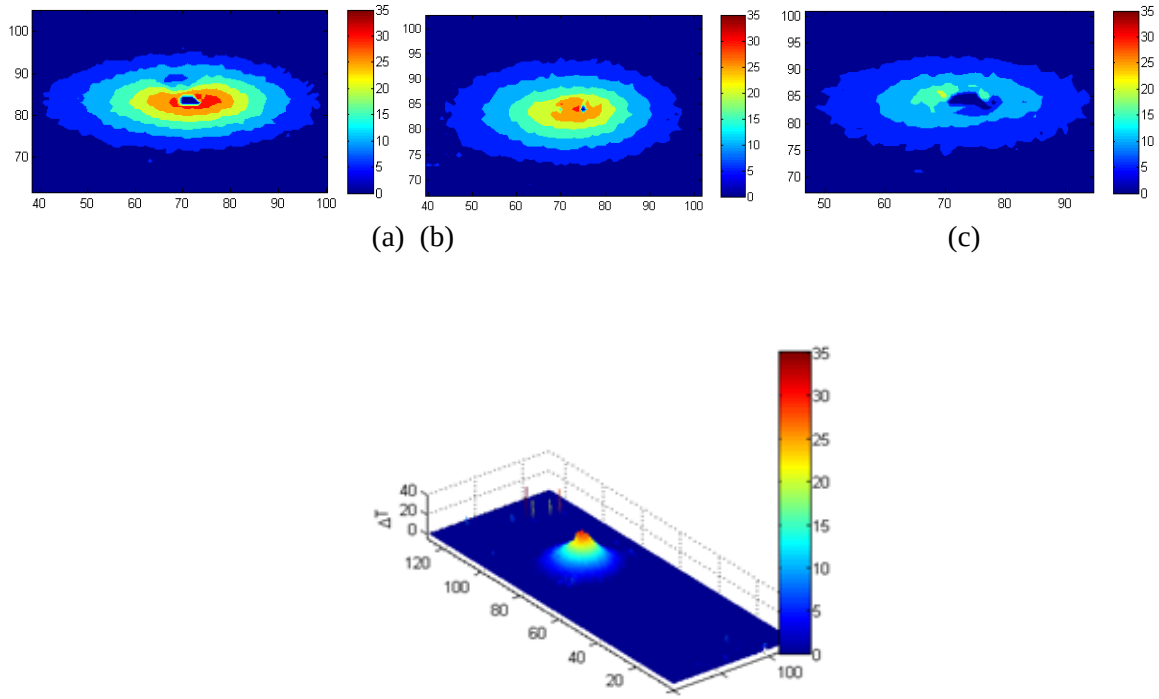

Figure 4.2. Temperature distribution of cross-sectional liver tissue. From left to right: a) The 9th slice (at the middle of the active tip), b) the 8th slice, and c) the 7th slice (close to the end of the active tip). d) A 3-D view of the temperature distribution of the 8th slice. The liver was irradiated with a power of 1.5 watts for 10 minutes.

The overall temporal profiles for temperature distribution at different positions with respect to diffuser tip are shown in Figure 4.2. The temperature 10 mm away from the diffuser tip is relatively low in comparison to that of other locations.

A gradual temperature distribution can be seen in Figure 4.4 along the horizontal and vertical lines of slice 8 with the highest temperature as the origin, immediately after laser irradiation.

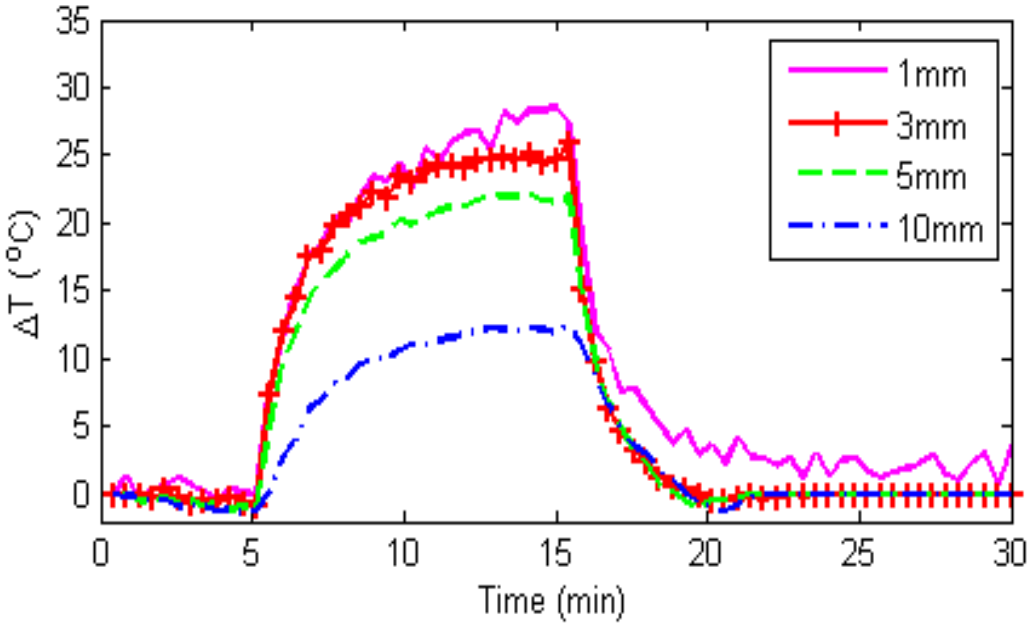

Figure 4.3. Temperature distribution in liver tissue at different distances with respect to the active tip during interstitial laser irradiation. The liver tissue was irradiated with a laser power of 1.5 watts for 10 minutes.

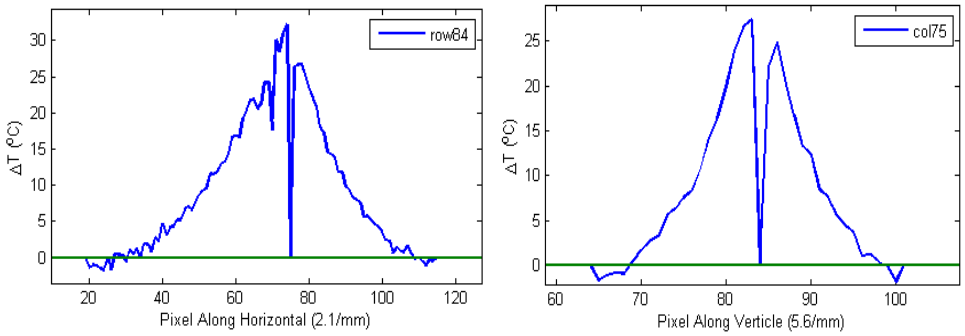

Figure 4.4. Temperature inside a liver tissue along the horizontal (a) and vertical (b) directions on the cross section of slide 8 with the highest temperature point in the tissue as the origin.

4.1.3 Temperature Profile of Rat Tumor

As described earlier, three different time lengths and power of laser irradiation were used for the treatment of rat tumor. The 3-D image was captured by MRI. Figure 4.5 shows the image

of a rat tumor before and after the laser irradiation of 1.65W for 10 min. The different color represents different temperatures.

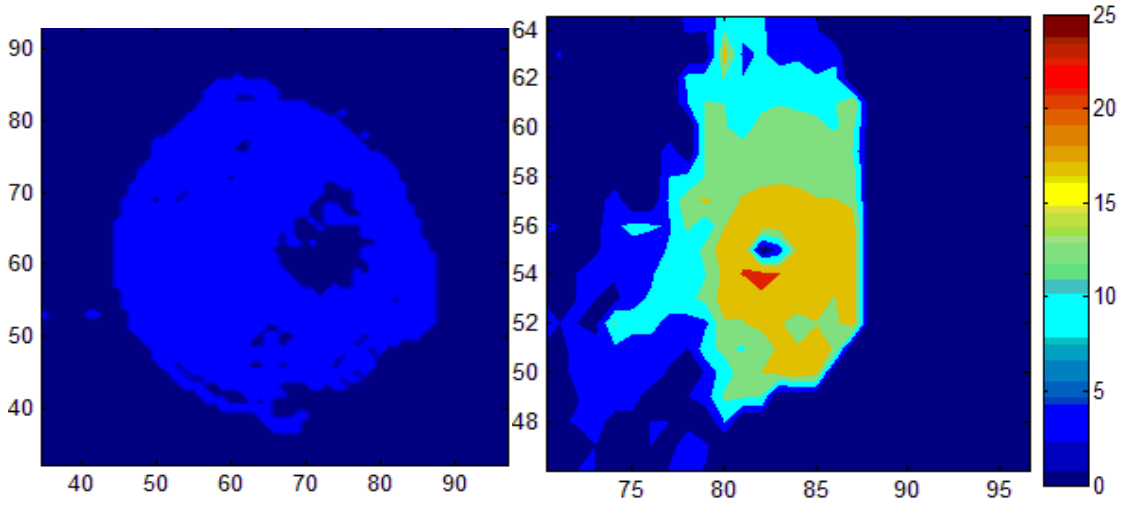

(a) (b)

Figure 4.5. MRI images of a rat tumor during interstitial laser treatment with a power of 1.65W. The figures depict the images before a) and after b) 10 minutes of laser irradiation.

Figure 4.6 shows the change in temperature inside of a tumor with respect to time at 1 mm distance from the active tip irradiated with 1.65 W for 10 min. The temperature increase was 18^{o}C compared to the initial temperature. The error around 10-15 min could be due to the motion artifact.

Figure 4.7 shows the change in temperature inside a tumor against time at a distance of 1 mm and 3 mm from the active diffuser tip when irradiated with 1.8 W for 30 min. At a distance of 1 mm, the change in temperature is higher compared to that at a distance of 3 mm.

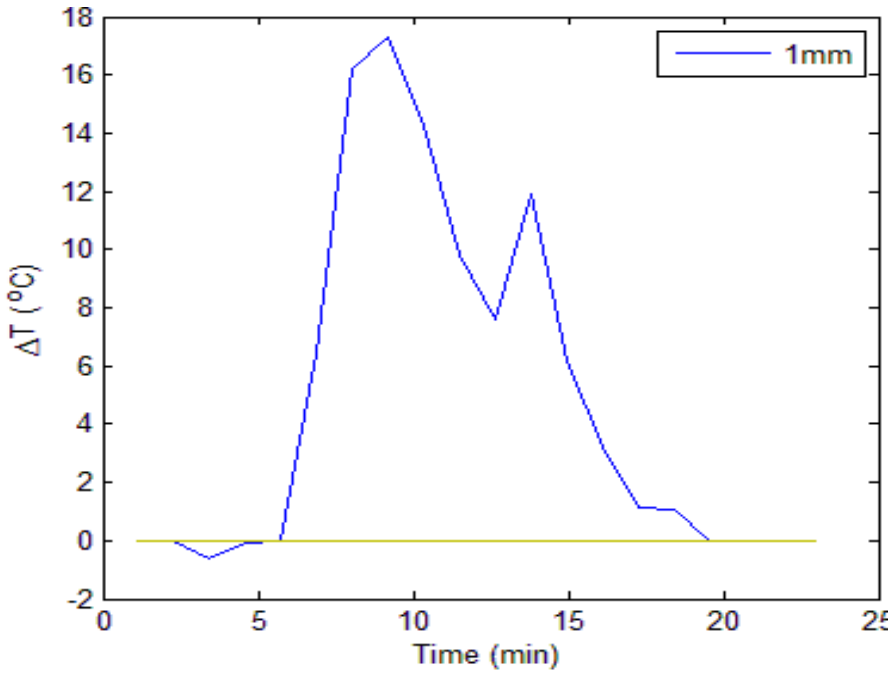

Figure 4.6. Temperature inside a tumor 1 mm away from the active tip as function of time. A temperature spike around 13 minutes is likely due to the motion artifact.

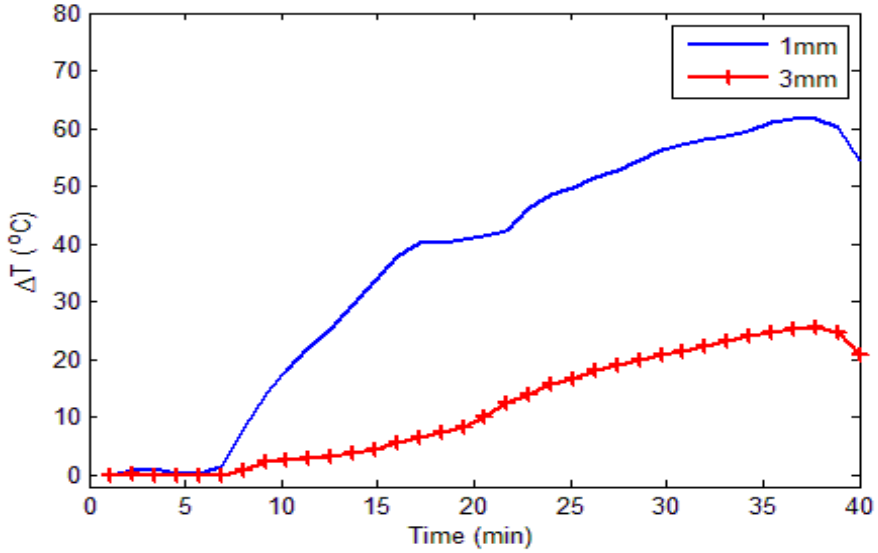

Figure 4.7. Temperature inside a tumor as function of time at the positions of 1 mm and 3 mm away from the active tip. The laser power is 1.8 watts. A large temperature difference was observed between the locations 2 mm apart at this power.

Comparing the temperature changes at time intervals of 10 min, 20 min and 30 min for both of these distances; we found the temperature changes to be 30^0C, 45^0C and 60^0C for 1mm and 5^0C, 15^0C and 25^0C for 3mm, respectively.

Figure 4.8 shows the temperature along two different axes on one slide after laser irradiation of 1.8W.

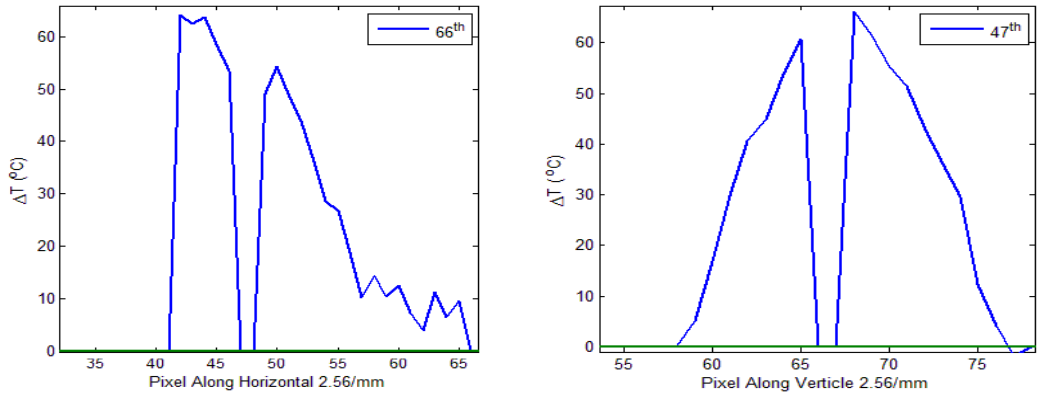

(a) (b)

Figure 4.8. Temperature inside a tumor along the vertical (a) and horizontal (b) axes of a selected slide after 10 min irradiation. Temperature drops sharply beyond 1mm. The laser power is 1.8 watts.

Figure 4.9 shows the thermal images of a rat tumor at different time intervals- 0 min, 10 min, 20 min and 30 min during a laser irradiation of 1.8W was used for 30 min. Laser irradiation caused high temperature increase with prolonged treatment. The region that was close to the fiber tip was very hot compared to the distant region. Hence, the temperature was found to be directly proportional to the time of laser irradiation whereas inversely proportional to the distance from the laser irradiation. The temperature in some hot regions was found to be almost 70^0C.

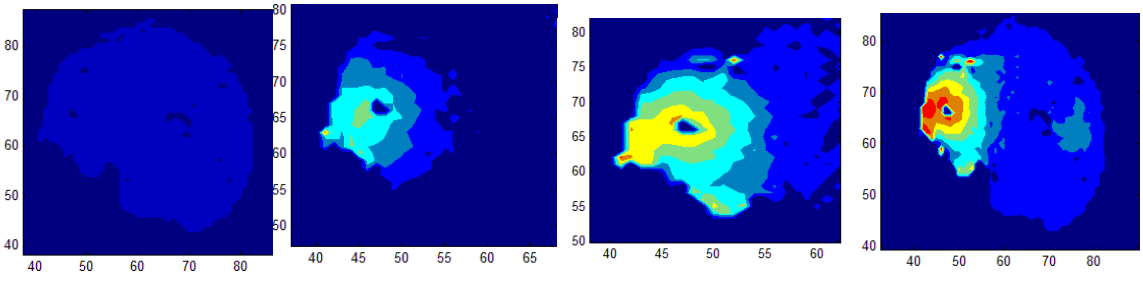

(a) (b) (c) (d)

Figure 4.9. Thermal images of a tumor during laser treatment with 1.8 watts. The figures depict the images for 0 (a), 10 (b), 20 (c), and 30 (d) minutes, into laser irradiation.

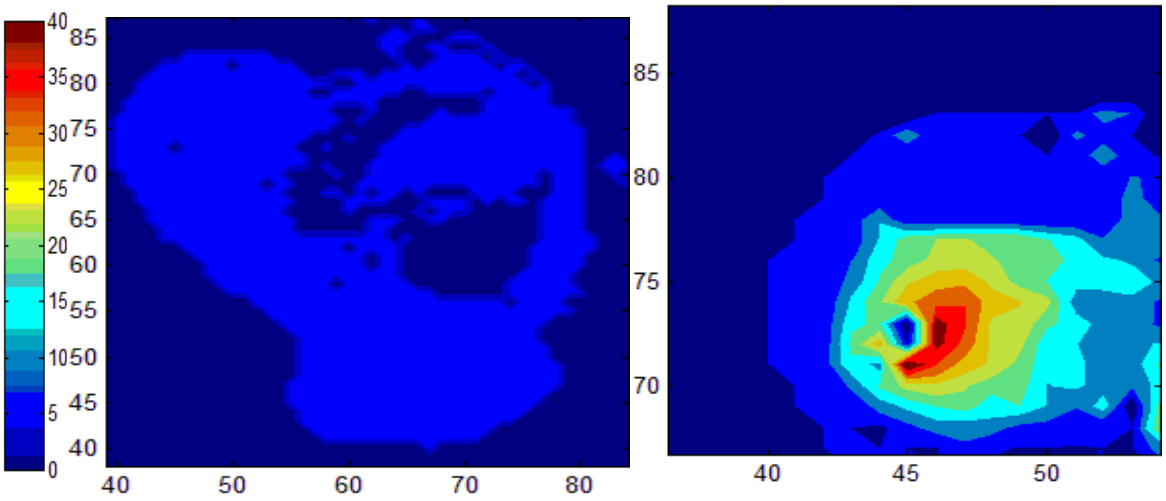

Figure 4.10. Thermal images of a tumor during laser treatment with 2.16W. The figures depict the images before (a) and after (b) 10-min laser irradiation.

With laser irradiation power of 2.16 W for 10 min, the temperature elevation was 28^{o}C 1 mm distance from active diffuser tip. Figure 4.10 shows the thermal image of rat tumor before and after the laser irradiation.

However, motion artifact contributed to noisy data beyond 2 mm, as shown in Figure 4.11. It is noted that the temperature range is similar to the 1.8 W at the 10 min mark.

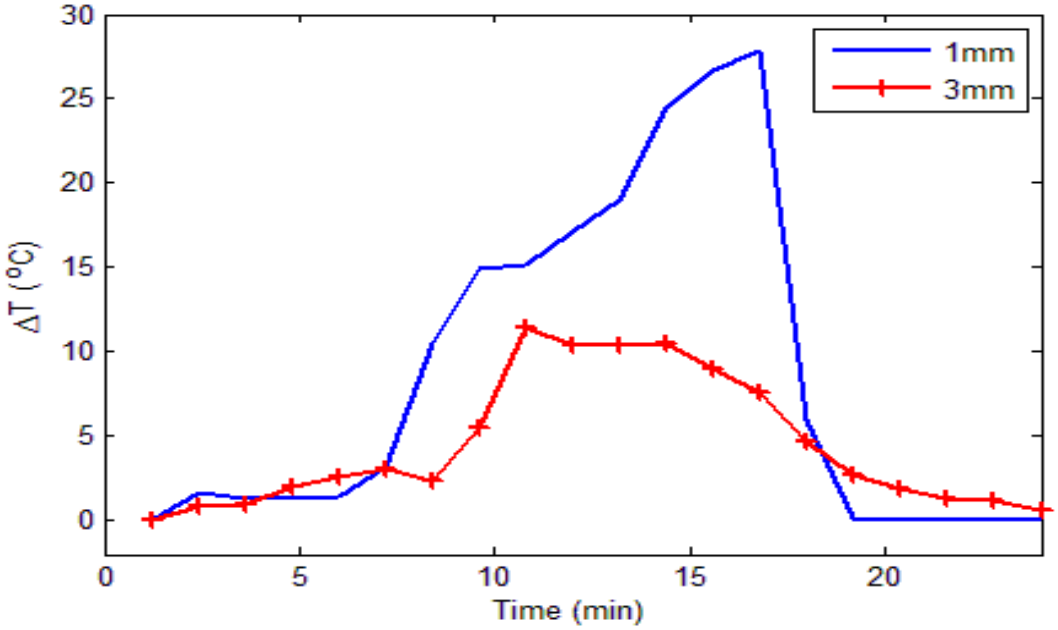

Figure 4.11. Temperature inside a tumor during laser treatment with 2.16W at different locations from the active tip of the cylindrical diffuser. The fluctuation of the data is due to the unstable respiration of the rat during the treatment.

4.2 Rat Temperature Measurement using Thermocouple

To compare the measurements using PRF with the thermocouple, we measured the temperature inside a rat tumor during laser irradiation. Thermocouple probes were placed 2 and 5 mm away from the active tip. With 1 and 1.5 W of laser power and 30-min irradiation using a 0.5-cm active tip, the temperature elevation reached a high level of 20-24^{o}C and 15-34^{o}C, respectively, as shown in Figure 4.12. Near saturation is seen under low power and longer irradiation time.

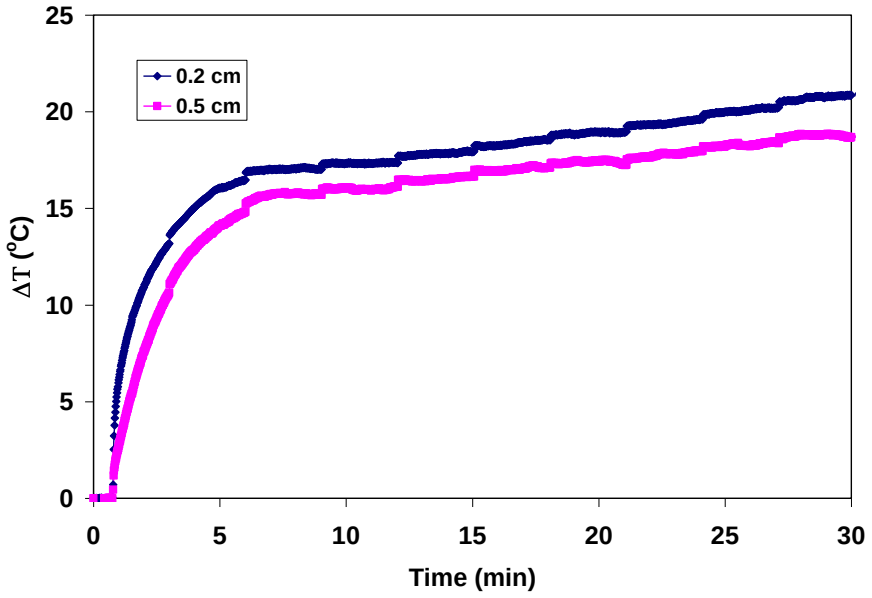

(a)

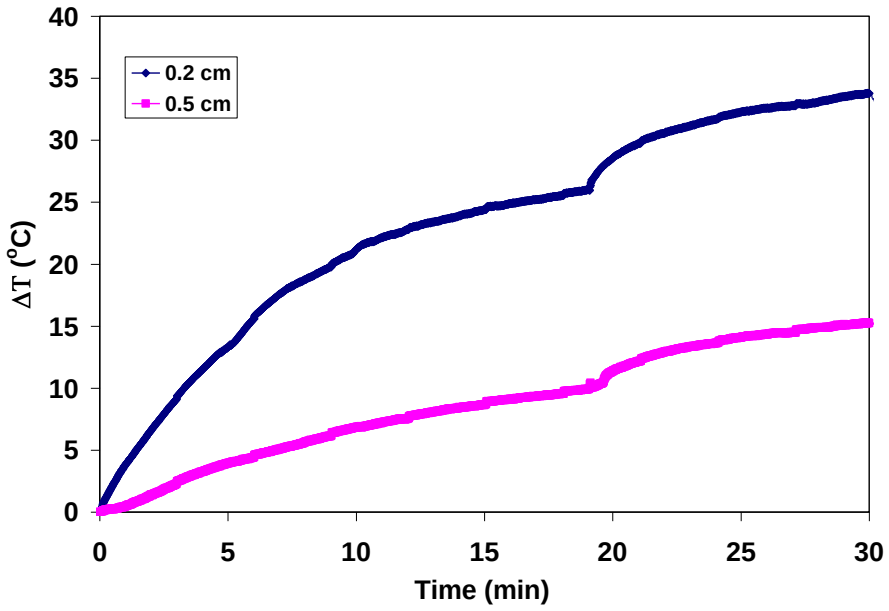

(b)

Figure 4.12. Temperature inside a tumor measured using thermocouple during laser irradiation using a 0.5-cm active tip with a laser power of 1 W (a) and 1.5 W (b).

4.3 TTC Staining of Tissue Damage

The TTC staining of treated tumor samples showed a cylindrical thermal damage zone with a ring of thermal necrosis around the fiber and with decreased thermal tissue interruption in the regions further away from the fiber tip as shown in Figure 4.13.

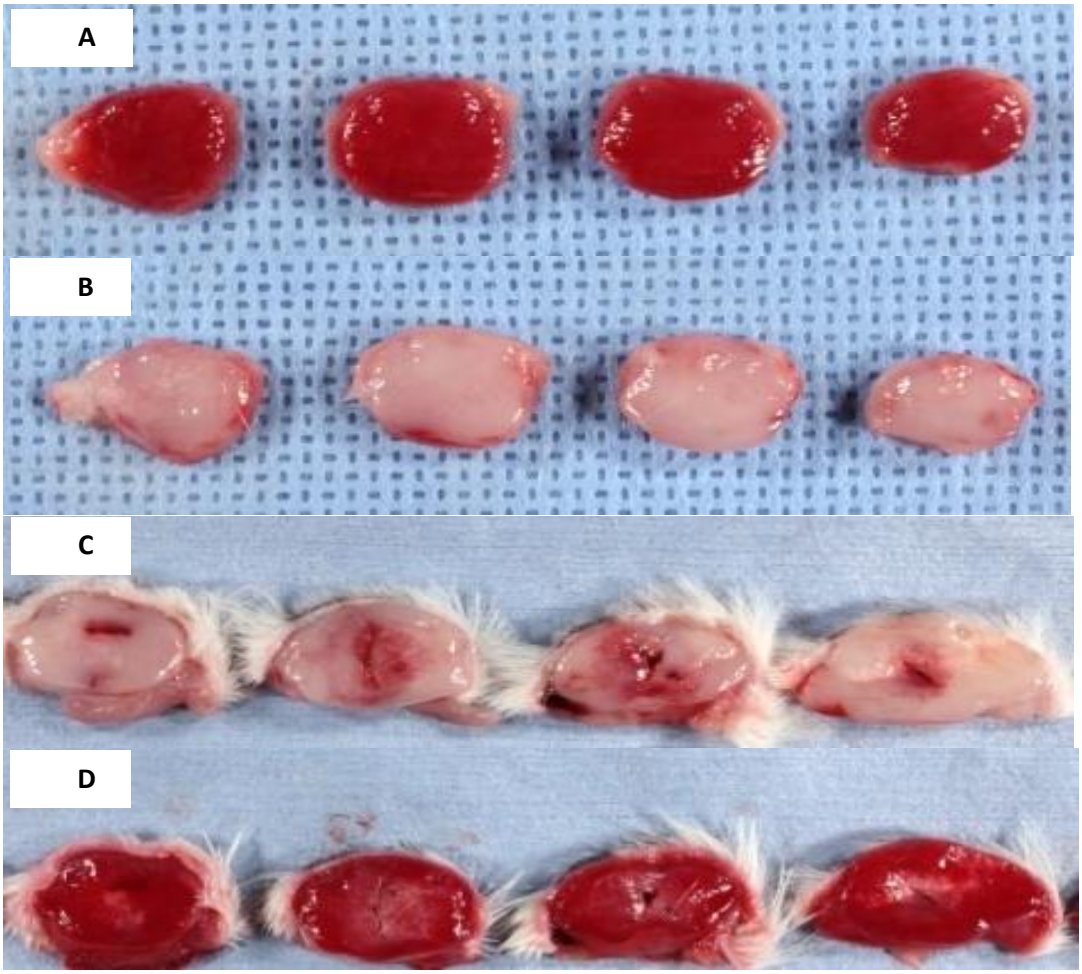

Figure 4.13. Tumor samples after interstitial laser irradiation. A cylindrical diffuser of 1-cm active length was placed in the center of the tumor. The tumor was irradiated with an output power of 1.5 watts for 10 minutes. The tumor sample was collected three hours after the laser irradiation. (A) Photo of a control tumor without treatment. (B) Photo of the control tumor in (A) after TTC staining. These control samples show uniform tissue structure (A) and uniform TTC staining (B), indicating a tumor sample with most viable tumor cells at the time of tissue collection. (C) Photo of a tumor after the interstitial irradiation. (D) Photo of the tumor in (C) after TTC staining. The treated tumor sample clearly showed the thermal damage (C) and also the death of tumor cells around the laser fiber (D).

4.4 Rat Survival

Figure 4.14 shows the combination of laser irradiation and immunostimulation resulted in the long-term survival of rats and prolonged survival time in treated groups. Particularly, the irradiations of 3 watts for 10 minutes and 2 watts for 30 minutes appear to be more effective than other laser parameters. The overall results in the Figure 4.14 show that interstitial laser immunotherapy can be effective in treating aggressive metastatic tumors.

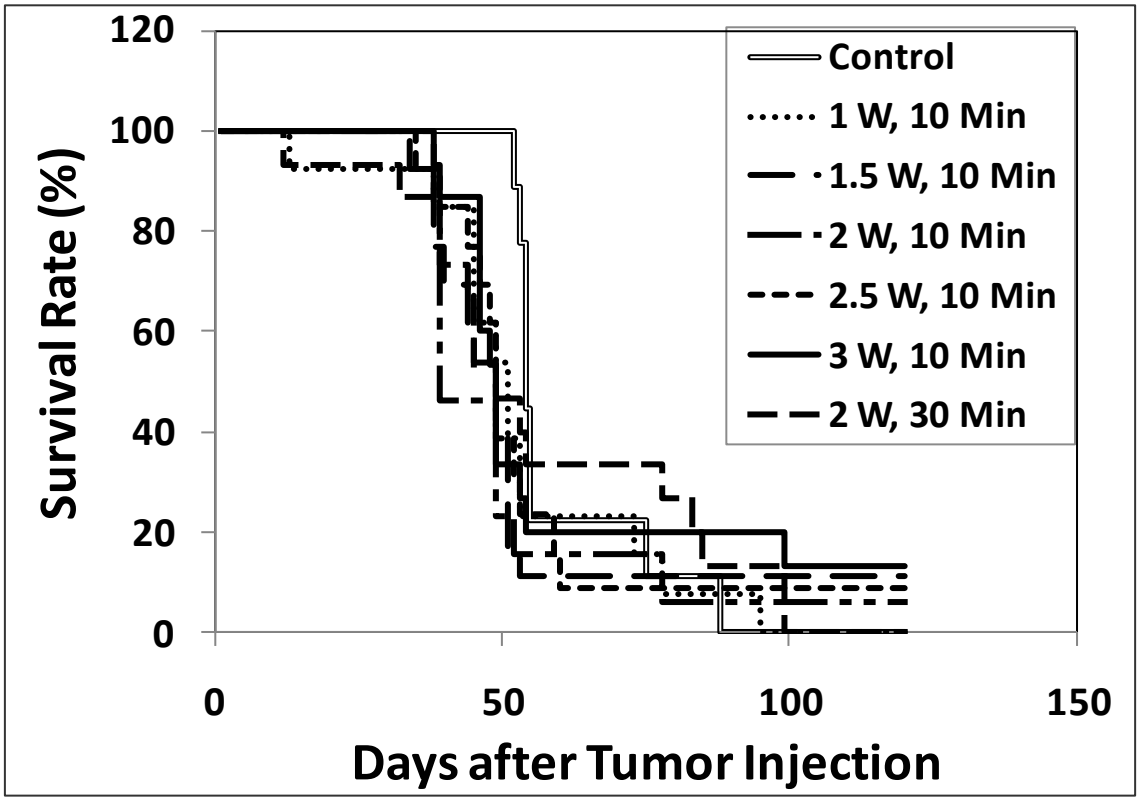

Figure 4.14. Survival plot of treated rats along with control group survival.

5. Discussion

In this study, ILIT has been found to be an effective therapy method of treating metastatic cancer. ILIT uses the concept of efficient laser irradiation to kill the tumor cells with the process known as photothermal interaction. The efficiency of laser irradiation is increased by concentrating the laser light deeply and directly into the tissue tumor without irradiating the surface. In addition, the photothermal interaction is enhanced immunologically using GC.

The laser light is delivered into the tumor tissue through a cylindrical tipped optical diffuser. Almost the entire laser energy is absorbed by the tumor cells. Whereas, when the laser light was irradiated on the surface, by the time it reached inside the tumor, much of the laser energy would have been lost to the intervening tissues between the skin and the tumor.

Photothermal phenomenon is an exciting topic in research and in clinical applications. The photothermal-tissue interaction alone can cause direct tissue damage. With appropriate laser parameters, this interaction can be used in a variety of clinical applications such as lesion ablation, resurfacing, and tissue welding. The thermal damage can also be used to treat tumors. However, due to the absorption of the laser energy by tissue, the direct use of the laser limits the effective treatment area only to the surface tissue or to the region in close vicinity of the laser source.

ILIT is an advanced form of LIT. In LIT therapy process, certain dyes were used so that most of the laser was absorbed by the target tissue. It turned out that even with dye enhancement the surface exposed to the laser light directly absorbed a large amount of laser energy.

The results of ILIT depend on temperature distribution and animal survival rates. Temperature distribution was one of the major concerns of ILIT, as we did not want to damage normal tissue. This part of study was focused on PRF temperature mapping with a known

measuring references. The calibration results using both PRF and optical sensors show the reliability of the temperature measurements. The homogeneous tissue composition in liver tissue allows for a smooth temperature gradient. In many cases, the temperature elevation decreases significantly at locations 1 mm or more away from the active tip of the cylindrical diffuser.

In our animal study, rats were divided into several groups and treated with different laser power for different durations. The survival rate of these different groups was studied. The groups that had the higher survival rate provided the clue as to which laser parameter could be the best as shown by the results in Figure 4.14.

The balance of power and irradiation duration is crucial in ILIT. Raising the power may only increase temperature 5mm away by a small amount. We have seen from our results in Figure 4.7 and Figure 4.11 that higher power (>1W) and /or longer duration of irradiation constitute a relatively broader thermal damage zone (>8^{o}C for a radius ≥3mm). For a typical tumor radius of ~5mm, 80-90% of the target area reached over 10^{o}C increase following higher power (>2W) and longer time (30 min) as shown by the results in Figure 4.7.

However, the temperature increase is not the overriding criterion for laser immunotherapy since the tumor antigen release may require an appropriate temperature increase for the thermal damage to tumor tissue.

While this current study focused on the thermal effects induced by interstitial laser irradiation, the biological effects induced by interstitial irradiation will be evaluated in the future, together with the application of the immunostimulant.

Variation in tissue composition not only affects the PRF results but also the temperature conductance. Abnormal temperature distribution is likely due to diversity in tissue composition including lipids, necrosis, and fluids. In these cases, a higher power or longer duration is needed to overcome these barriers. Nevertheless, moderate power and duration may be the best solutions in terms of biological and thermal interactions.

The LIT method used earlier may not be optimal. Care must be taken when administering treatment to large tumors. It is worth noting that the beauty of ILIT is that it does not need to completely destroy all tumor cells in order to stimulate an effective immune response.

Signal intensity and respiration stability are significant indicators of the quality and reliability of PRF measurements as shown by the results in Figure 4.6. Physical target size is also an important factor for imaging in terms of resolution. Due to a finite spatial resolution, the tumor size cannot be too small for a reliable assessment.

Understanding how laser and tissue interact is one of the key factors to a better treatment outcome, particularly in laser immunotherapy, since an increase in temperature is crucial for tumor destruction and antigen release. We have shown in this study that ILIT can be an effective modality to induce desirable photothermal damage to tissue. We also demonstrated that together with application of immunoadjuvant, ILIT can be used to treat metastatic tumors. More importantly, this study demonstrated that the effectiveness of ILIT can be monitored by magnetic resonance imaging using PRF. Future studies will focus on improving our spatial and temporal resolutions. Furthermore, we will conduct more animal studies using ILIT for the treatment of metastatic tumors.

6. References

1. R.L. Klein, A.R. Brown, C.M. Castro, S.K. Chambers, J.M. Cragun, L.G. LeBeau and J.E. Lang, "Ovarian Cancer Metastatic to the Breast Presenting as Inflammatory Breast Cancer: A Case Report and Literature Review," Journal of Cancer 1:27-31 (2010).
2. W.R. Chen, R. Carubelli, H. Liu and Nordquist, "Laser Immunotherapy: A Novel Treatment Modality for Metastatic Tumors," Molecular Biotechnology 25:37-43 (2003).
3. W.R. Chen, S. Jeong, M. Lucroy, R. Wolf, E. Howard, H. Liu and R. Nordquist, "Induced anti-tumor immunity against DMBA-4 metastatic mammary tumors in rats using a novel approach," International Journal of Cancer 107 (6): 1053-1057 (2003).
4. W.R. Chen, M. Korbelik, K. Bartels, H. Liu, J. Sun and R. Nordquist, "Enhancement of laser cancer treatment by a chitosan-derived immunoadjuvant," Photochemistry and Photobiology 81: 190-195 (2005).
5. S.H. Giordano, D.S. Cohen, A.U. Buzdar, G. Perkins and G.N. Hortobagyi, "Breast carcinoma in men: A population-based study," Cancer 101: 51-57 (2004).
6. W.F. Anderson, R.M. Pfeiffer, G.M. Dores and M.E. Sherman, "Comparison of age frequency distribution patterns for different histopathologic types of breast carcinoma," cancer Epidemiol Biomarkers 15: 1899-1905 (2006).
7. C. Carlomagno, A. Farella, L. Buccci, F.P. D'Armiento, G. Pesce, S. Pepe, L. Cannella, R. Pacelli, A.D. Stefano, R. Solla, M.R. D'Armiento and S. De Placido, "Neo-adjuvant treatment of rectal cancer with capecitabine and oxaliplatin in combination with radiotherapy: a phase II study," Ann Oncol: 719 (2009).
8. D.I. Rosenthal, P.J. Catalano, D. Haller, J.C. Landry, E.R. Sigurdson, F.R. Spitz and A.B. Benson, "Phase I study of preoperative radiation therapy with concurrent infusional 5-

fluorouracil and oxaliplatin followed by surgery and postoperative 5-fluorouracil plus leucovorin for T3/T4 rectal adenocarcinoma," ECOG E1297. Int J Radiat Oncol Biol Phys 72: 108–13 (2008).

9. A.T. Shivnani, Jr. W. Small, S.J. Stryker, K.D. Kiel, S. Lim, A.L. Haverson and M.S. Talaminti, "Preoperative chemoradiation for rectal cancer: results of multimodality management and analysis of prognostic factors," Am JSurg 193:389–93 (2007).
10. J.L. Lefebvre, F. Rolland, M. Tesselaar, E. Bardet, C.R. Leemans, L. Geoffrois, P. Hupperets, L. BArzan, D. Raucourt, D. Chevalier, L. Licitra, F. Lunghi, R. Stupp, D. Lacombe, J. Bogaerts, J.C. Horiot, J. Bernier and J.B. Vermorken, "Phase 3 randomized trial on larynx preservation comparing sequential vs. alternating chemotherapy and radiotherapy," J Natl Cancer Inst: 460 (2009).
11. M. Posner and J.B. Vermorken, "Induction therapy in the modern era of combinedmodality therapy for locally advanced head and neck cancer," Semin Oncol 35:221–8 (2008).
12. K. Nagai, R. Tsuchiya and T. Mori, H. Tada, Y. Ichinose, T. Koike and H. Kato, Lung cancer surgical study group of the Japan clinical oncology group, "A randomized trial comparing induction chemotherapy followed by surgery with surgery alone for patients with stage IIIA N2 non-small cell lung cancer," J Thorac Cardiovasc Surg 125: 254–60 (2003).
13. I. Chau, G. Brown, D. Cunningham, D. Tait, A. Wotherspoon, A.R. Norman, N. Tebbutt, M. Hill, P.J. Ross, A. Massey and J. Oates, "Neoadjuvant capecitabine and oxaliplatin followed by synchronous chemoradiation and total mesorectal excision in magnetic resonance imaging-defined poor-risk rectal cancer," J Clin Oncol 24:668–74 (2006).

14. Wei R. Chen, Hong Liu, Jerry W. Ritchey, Kenneth E. Bartels, Michael D. Lucroy and Robert E. Nordquist, "Effect of Different Components of Laser Immunotherapy in Treatment of Metastatic Tumors in Rats1," Cancer Research 62:4295-4299 (2002).

15. W.R. Chen, R.L. Adams, R. Carubelli, and R.E. Nordquist, "Laser-photosensitizer assisted immunotherapy: A novel modality in cancer treatment," Cancer Lett. 115: 25-30, (1997).

16. W.R. Chen, R. Carubelli, H. Liu and R.E. Nordquist," Laser Immunotherapy: A Novel Treatment Modality for Metastatic Tumors," Mol. Biotechnol 25: 37-43 (2003).

17. J.L. Boulnois, "Photophysical processes in recent medical laser developments: a review," Lasers Med Sci. **1**: 47-66 (1986).

18. S.L. Jacques, "Laser-tissue interactions," The Cancer Bulletin 41: 211-218 (1989).

19. S. Thomsen, "Pathologic analysis of photothermal and photomechanical effects of laser-tissue interactions," Photochem Photobiol. 53: 825-835 (1991).

20. S.L. Jacques, "Laser-tissue interactions. Photochemical, photothermal, and photomechanical," Surg. Clin. North Am **72**: 531-558 (1992).

21. T.J. Dougherty, J.E. Kaufman, A. Goldfarb, K.R. Weishaupt, D.G. Boyle and A. Mlttleman, "Photoradiation therapy for the treatment of malignant tumors," Cancer Research 38: 2628-2635 (1978).

22. M.J. Manyak, A. Russo, P.D. Smith and E. Glatsein. "Photodynamic therapy," J. Clin. Oncol. 6:380-391 (1988).

23. T.J. Dougherty, "Photoradiation therapy for cutaneous and subcutaneous malignancies," J. Invest. Dermatol. **77**:122-124 (1981).

24. A. Dahlman, "Laser photoradiation therapy of cancer," Cancer Research 43**:** 430-434 (1983).

25. T.J. Dougherty, “Photodynamic therapy: status and potential,” Oncology 3**:** 67-78 (1989).

26. S.L. Marcus, "Photodynamic therapy of human cancer: clinical status, potential and needs," Future Directions and Applications in Photodynamic Therapy (C.J. Gomer, eds.), 5:56, SP IE Press, Bellingham, WA (1990).

27. N.A. Buskard “The use of photodynamic therapy in cancer,” Seminars in Oncology 21: 1-27 (1994).

28. A.M. Fisher, A.L. Murphee and C.J. Gomer, “Clinical and pre-clinical photodynamic therapy,” Lasers Surg. Med. 17: 2-31 (1995).

29. W.R. Chen, R.L. Adams, R. Carubelli and R.E. Nordquist, “Laser-photosensitizer assisted immunotherapy: A novel modality in cancer treatment,” Cancer Lett. 115: 25-30 (1997).

30. W.R. Chen, W. Zhu, J. Dynlacht, H. Liu and R. Nordquist, “Long-term tumor resistance induced by laser photo-immunotherapy,” International Journal of Cancer 81: 808-812 (1999).

31. W.R. Chen, A. Singhal, H. Liu and R. Nordquist, “Laser immunotherapy induced antitumor immunity and its adoptive transfer,” Cancer Research 61: 459-461 (2001).

32. W.R. Chen, Jerry W. Ritchey, Kenneth E. Bartels, Hong Liu and R. Nordquist, “Effect of different components of laser immunotherapy in treatment of metastatic tumors in rats,” CancerResearch 62: 4295-4299 (2002).

33. W.R. Chen, S. Jeong, M. Lucroy, R. Wolf, E. Howard, H. Liu and R. Nordquist, “Induced anti-tumor immunity against DMBA-4 metastatic mammary tumors in rats using a novel approach,” International Journal of Cancer 107:1053-1057 (2003).

34. W.R. Chen, M. Korbelik, K. Bartels, H. Liu, J. Sun and R. Nordquist, "Enhancement of laser cancer treatment by a chitosan-derived immunoadjuvant," Photochemistry and Photobiology 81:190-195 (2005).

35. C.W. Song, A. Lokshina, J. G. Rhee, M. Patten and S.H. Levitt, "Implication of blood flow in hyperthermic treatment of tumors. IEEE Trans," Biomed. Engin. 31:9-16 (1984).

36. H.S. Reinhold and B. Endrich, "Tumour microcirculation as a target for hyperthermia," Int. J.Hypertherm. 2:111-137 (1986).

37. C.W. Song, H. J. Park, C. K. Lee and R. Griffin., "Implications of increased tumor blood flow and oxygenation caused by mild temperature hyperthermia in tumor treatment," Int. J. Hyperthermia 21:761-767 (2005).

38. C.W. Song, L. M. Chelstrom, S.H. Levitt and D. J. Haumschild, "Effects of temperature on blood circulation measured with the laser Doppler method," Int. J. Radiat. Oncol. Biol. Phys.17:1041-1047 (1989)

39. A.J. Thistlethwaite, D. B. Leeper, D. J. Moylan and R. E. Nerlinger, "pH distribution in human tumors," Int. J. Radiat. Oncol. Biol. Phys. 11:1647-1652 (1985).

40. W.C. Dewey, L. E. Hopwood, S. A. Sapareto and L. E. Gerweck., "Cellular responses to combinations of hyperthermia and radiation," Radiology 123:463-474 (1977).

41. J. Overgaard, "Simultaneous and sequential hyperthermia and radiation treatment of an experimental tumor and its surrounding normal tissue in vivo," Int. J. Radiat. Oncol. Biol. Phys. 11:1507-1517 (1980).

42. G. Arcangeli, A. Cividalli, C. Nervi, G. Creton and G. Lovisolo, "Tumor control and therapeutic gain with different schedules of combine radiotherapy and local external hyperthermia in human cancer," Int. J. Radiat. Oncol. Biol. Phys. 8: 1125-1134 (1983).

43. S.B. Field and C. C. Morris, “The relationship between heating time and temperature: its relevance to clinical hyperthermia. Radiother,” Oncol. 1:179-186 (1983).

44. S.A. Sapareto and W. C. Dewey, “Thermal dose determination in cancer therapy,” Int. J.Radiat. Oncol. Biol. Phys. 10:787-800 (1984).

45. B.V. Harmon, A.M. Corder, R.J. Collins, G.C. Gobe, J. Allen, D.J. Allan and J.F. Kerr “Cell Death Induced in a Murine Mastocytoma by 42- 47°C Heating in Vitro: Evidence that the Form of Death Changes from Apoptosis to Necrosis Above a Critical Heat Load,” Int. J. Radiat. Biol. 58: 845-858 (1990).

46. L.J. Anghileri and J. Robert, “Hyperthermia in cancer treatment,” CRC Press. Boca Raton, FL (1986).

47. J.A. Dickson and S. K. Calderwood, “Temperature Range and Selective Sensitivity of Tumors to Hyperthermia: A Critical Review, “Annals of the New York Academy of Sciences, 335: 180–205 (1980).

48. J. De Poorter, C. de Wagter, Y. de Deene, C. Thomsen, F. Stahlberg and E. Achten, “Noninvasive MRI thermometry with the proton resonance frequency (PRF) method: in vivo results in human muscle,” Magn Reson Med 33 74-81 (1995).

49. Q. Bruno, J.A. de Zwart and C.T.W. Woonen, “Magnetic Resonance Temperature Imaging for Guidance of Thermotherapy,” Journal of Magnetic Resonance Imaging 12, 525-533 (2000).

50. J.C. Hindman, “Proton resonance shift of water in the gas and liquid states,” J. Chem Phys. 44(12): 4582-92 (1966).

51. K. Kuroda, “Temperature Mapping Using the Water Proton Chemical Shift: A Chemical Shift Selective Phase Mapping Method,” Magn Reson Med. 38(5): 845-51 (1997).

52. R. Stollberger, P.W. Ascher, D. Huber, W. Renhart, H. Radner and F. Ebner, “Temperature monitoring of interstitial thermal tissue coagulation using MR phase images” J Magn Reson Imag 8: 188-196 (1998)

53. J. Olsrud, R. Wirestam, S. Brockstedt, A.M.K. Nilsson, K.G. Tranberg, F. Stahlberg and B.R.R. Persson, “MRI thermometry in phantoms by use of the proton resonance frequency shift method: application to interstitial laser thermotherapy,” Phys Med Biol 43: 2597-2613 (1998).

54. S.C. Gnyawali, Y. Chen, F. Wu, K.E. Bartels, J.P. Wicksted, H. Liu and W.R. Chen, “Temperature Measurement on Tissue Surface during Laser Irradiation”, Medical and Biological Engineering and Computing,” 46:159-168 (2008).

55. Y. Chen, S.C. Gnyawali, F. Wu, H. Liu, Y.A. Tesiram, A. Abbott, R.A. Towner and W.R. Chen, “Magnetic resonance imaging guidance for laser photothermal therapy”, Journal of Biomedical Optics **13:** 044033 (2008).

56. T. Kahn, T. Harth, J.C. Kiwit, H.J Schwarzmaier, C. Wald and U. Mödder, “In vivo MRI thermometry using a phase-sensitive sequence: Preliminary experience during MRI-guided laser induced interstitial thermotherapy of brain tumors,” J Magn Reson Imag 8: 160-164 (1998).

57. M. Naylor, W. Chen, T.K. Teague, L. Perry and R. Nordquist. 2006. “In Situ Photo Immunotherapy: A Tumor-Directed Treatment Modality for Melanoma,” British Journal of Dermatology 155: 1287-1292.

58. X. Li, M. Naylor, R. Nordquist, T.K. Teague, H. Le, C.A. Howard, C. Murray and W.R. Chen, “Clinical effects of in situ Photoimmunotherapy on late-stage melanoma patients: a preliminary study,” Cancer Biology and Therapy 10:1077-1214 (2010).

59. X. Li, T. Hode, M.C. Guerra, G. L. Ferrel, J.A. Lunn, O. Adalsteinsson, R.E. Nordquist and W.R. Chen, “Combined effects of selective photothermal therapy and immunoadjuvant against Stage IV breast cancer,” Journal of Innovative Optical Health Science 3: 279-284 (2010).

60. X. Li, G.L. Ferrel, M.C. Guerra, T. Hode, J.A. Lunn, O. Adalsteinsson, R.E. Norquist, H. Liu and W.R. Chen “Preliminary safety and efficacy results of laser immunotherapy for the treatment of metastatic breast cancer patients,” Photochemical and Photobiological Sciences. In press (2011).

61. Hendee, William R; Morgan and J. Christopher, "Magnetic Resonance Imaging Part I—Physical Principles," West J Med. 141 (4): 491–500 (1984).

62. PC. Lauterbur, "Image Formation by Induced Local Interactions: Examples of Employing Nuclear Magnetic Resonance," Nature 242 (5394): 190–191 (1973).

63. R. Damadian, M. Goldsmith and L. Minkoff, "NMR in cancer: XVI. Fonar image of the live human body," Physiological Chemistry and Physics 9: 97–100 (1977).

64. D. Le Bihan, E. Breton, D. Lallemand, P. Grenier, E. Cabanis and M. Laval-Jeantet, "MR imaging of intravoxel incoherent motions: Application to diffusion and perfusion in neurologic disorders," Radiology. 161 (2): 401–7 (1986).

65. M.E. Moseley, Y. Cohen, J. Mintorovitch, L. Chileuitt, H. Shimizu, J. Kucharczyk, M.F. Wendland and P.R. Weinstein, "Early detection of regional cerebral ischemia in cats:

Comparison of diffusion- and T_2-weighted MRI and spectroscopy," Magn Reson Med 14 (2): 330–46 (1990).

66. J.P. Ridgway and M.A. Smith, "A technique for velocity imaging using magnetic resonance imaging," Br J Radiol 59 (702): 603–7 (1986).

67. W. Golder, "Magnetic resonance spectroscopy in clinical oncology," Onkologie 27 (3): 304–9 (2007).

68. K.R. Thulborn, J.C. Waterton, P.M. Matthews and G.K. Radda, "Oxygenation dependence of the transverse relaxation time of water protons in whole blood at high field," Biochim. Biophys. Acta 714 (2):265–70 (1982).

69. M. Brant-Zawadzki, G.D. Gillan and W.R. Nitz, "MP RAGE: A three-dimensional, T_1-weighted, gradient-echo sequence—initial experience in the brain," Radiology 182 (3): 769–75 (1992).

70. M.D. Deck, C. Henschke, B.C. Lee, R.D. Zimmerman, R.A. Hyman, J. Edwards, L.A. Saint Louis, P.T. Cahill, H. Stein and J.P. Whalen, "Computed tomography versus magnetic resonance imaging of the brain. A collaborative interinstitutional study," Clin Imaging 13 (1): 2–15 (1989).

71. D.L. Price, J.P. de Wilde, A.M. Papadaki, J.S. Curran and R.I. Kitney, "Investigation of acoustic noise on 15 MRI scanners from 0.2 T to 3 T," Journal of Magnetic Resonance Imaging 13 (2):288–293 (2001).

72. E. Kanal, A.J. Barkovich, C. Bell, J.P. Borgstede, W.G. Bradley, J.W. Froelich, T. Gilk, J.R. Gimbel, J. Gosbee, E.K. Kaminski, J.W. Lester, J. Nyenhuis, Y. Parag, D.J. Schaefer, E.A.S. Scoumis, J. Weinreb, L.A. Zaremba, P. Wilcox, L. Lucey and N. Sass, "ACR Guidance Document for Safe MR Practices," AJR Am J Roentgenol. 188 (6):1–27 (2007)

73. FDA Drug Safety Communication, “New warnings for using gadolinium-based contrast agents in patients with kidney dysfunction," Information on Gadolinium-Based Contrast Agents. U.S. Food and Drug Administration (2010).

74. “Assessment of electromagnetic fields around magnetic resonance (MRI) equipment,” MCL-T Ltd, London, RR570 (2007)

75. Carr, Herman, "Letter: Field Gradients in Early MRI," Physics Today 57 (7): 83 (2004).

76. M.W. Dewhirst, W.G. Conner, T.E. Moon and H.B. Roth, “Response of spontaneous animal tumors to heat and/or radiation: preliminary results of a phase III trial,” J. Natl. Cancer Inst. 61:395-397 (1982).

77. H.H. Leveen, S. Wapnick, V. Riccone, G. Falk and N. Ahmed, “Tumor eradication by radio-frequency therapy,” J. Am. Med. Assoc. 235:2198-2200 (1976).

78. M.R. Manning, T.C. Cetas, R.C. Miller, J.R. Oleson, W.G. Conner and E.W. Gerner, “Results of a phase I trial employing hyperthermia alone or in combination with external beam or interstitial radiotherapy,” Cancer 49:205-216 (1982).

79. J.B. Marmor, D. Pounds, D.B. Postic and G.M. Hahn, “Treatment of superficial human neoplasms by local hyperthermia induced by ultrasound,” Cancer 43:196-205 (1979).

80. E. Jager, D. Jager and A. Knuth, “Antigen-specific immunotherapy and cancer vaccines,” Int. J. Cancer. 106:820-817 (2003).

81. A. Mukhopadhaya, J. Mendecki, X. Dong, L. Liu, S. Kalnicki, M. Garg, A. Alfieri and C. Guha, “Localized hyperthermia combined with intratumoral dendritic cells induces systemic antitumor immunity,” Cancer Res. 67:7798-7806 (2007).

82. P.K. Chakravarty, A. Alfieri, E.K. Thomas, V. Beri, K.E. Tanaka, B. Vikram and C. Guha, "Flt3-ligand administration after radiation therapy prolongs survival in a murine model of metastatic lung cancer," Cancer Res. 59:6028-6032 (1999).

83. P.K. Chakravarty, C. Guha, A. Alfieri, V. Beri, Z. Niazova, N.J. Deb, Z. Fan, E.K. Thomas and B. Vikram, "Flt3L therapy following localized tumor irradiation generates long-term protective immune response in metastatic lung cancer: its implication in designing a vaccination strategy," Oncology 70:245-254 (2006).

84. J. Guo, J. Zhu, X. Sheng, X. Wang, L. Qu, Y. Han, Y. Liu, H. Zhang, L. Huo, S. Zhang, B. Lin and Z. Yang, "Intratumoral injection of dendritic cells in combination with local hyperthermia induces systemic antitumor effect in patients with advanced melanoma," Int. J. Cancer 120**:**2418-2425 (2007).

85. K. Tanaka, A. Ito, T. Kobayashi, T. Kawamura, S. Shimada, K. Matsumoto, T. Saida and H. Honda, "Intratumoral injection of immature dendritic cells enhances antitumor effect of hyperthermia using magnetic nanoparticles," Int. J. Cancer 116:624-633 (2005).

86. M.H. den Brok, R.P. Sutmuller, S. Nierkens, E.J. Bennink, L.W. Toonen, C.G. Figdor, T.J. Ruers and G.J. Adema, "Synergy between in situ cryoablation and TLR9 stimulation results in a highly effective *in vivo* dendritic cell vaccine," Cancer Res. 66:7285-7292 (2006).